

Influence of combined compressor and turbine deterioration on the overall performance of a jet engine using RANS simulation and Pseudo Bond Graph approach

Original article

Article history:

Submission date: 29 September 2020

Acceptance date: 2 December 2020

Publication date: 22 December 2020

This is the updated version of a paper originally presented at the Global Power and Propulsion Virtual Technical Conference, GPPS Chania20, Sept. 7–9, 2020.



*Correspondence:

JG: j.goeing@ifas.tu-braunschweig.de

Peer review:

Single blind

Copyright:

© 2020 Goeing et al. © This is an open access article distributed under the Creative Commons Attribution License (CC-BY 4.0), which permits unrestricted use, distribution, and reproduction in any medium, provided the original work is properly cited and its authors credited.

Keywords:

CFD; jet engine; performance simulation; Bond Graph Theory; RANS simulation; maintenance repair and overhaul (MRO)

Citation:

Goeing J., Seehausen H., Pak V., Lueck S., Seume J. R., and Friedrichs J. (2020). Influence of combined compressor and turbine deterioration on the overall performance of a jet engine using RANS simulation and Pseudo Bond Graph approach. *Journal of the Global Power and Propulsion Society*. 4: 296–308.
<https://doi.org/10.33737/jgpps/131109>

Jan Goeing^{1*}, Hendrik Seehausen², Vladislav Pak², Sebastian Lueck¹, Joerg R. Seume², Jens Friedrichs¹

¹*Institute of Jet Propulsion and Turbomachinery, Technische Universitaet Braunschweig, Braunschweig, Lower Saxony, Germany*

²*Institute of Turbomachinery and Fluid Dynamics, Leibniz Universitaet Hannover, Garbsen, Lower Saxony, Germany*

Abstract

In this study, numerical models are used to analyse the influence of isolated component deterioration as well as the combination of miscellaneous deteriorated components on the transient performance of a high-bypass jet engine. For this purpose, the aerodynamic impact of major degradation effects in a high-pressure compressor (HPC) and turbine (HPT) is modelled and simulated by using 3D CFD (Computational Fluid Dynamics). The impact on overall jet engine performance is then modelled using an 1D Reduced Order Model (ROM).

Initially, the HPC performance is investigated with a typical level of roughness on vanes and blades and the HPT performance with an increasing tip clearance. Subsequently, the overall performance of the jet engines with the isolated and combined deteriorated domains is computed by the in-house 1D performance tool ASTOR (AircraftEngine Simulation for Transient Operation Research). Degradations have a significant influence on the system stability and transient effects. In ASTOR, a system of differential equations including the equations of motion and further ordinary differential equations is solved. Compared to common ROMs, this enables a higher degree of accuracy.

The results of temperature downstream of the high-pressure compressor and low-pressure turbine as well as the specific fuel composition and the HP rotational speed are used to estimate the degree and type of engine deterioration. However, the consideration of the system stability is necessary to analyse the characterisation in more detail.

Finally, a simplified model which merges two engines with individual deteriorated domains into one combined deteriorated engine, is proposed. The simplified model predicts the performance of an engine which has been simulated with combined deteriorated components.

Introduction

The degradation of jet engines results in performance losses, higher emissions, decreasing safety limits, and shortening of life cycles. An effective and accurate regeneration or recovery of a component can significantly reduce operating costs as well as the risk of failure. Therefore, the Collaborative Research Centre 871 “Regeneration of Complex Capital Goods” (CRC 871) develops a scientific basis for novel technologies and approaches to analyse and determine the causes and effects of wear.



Hence, these methods are exemplified using the V2500-A1, a mature high-bypass turbofan jet engine operated by the Institute of Jet Propulsion and Turbomachinery (IFAS) (Spuhler et al., 2019). In the CRC 871, the full regeneration process is formed by a real and a virtual repair process (Denkena et al., 2019). Therefore, many sub projects are working together to produce a digital twin of a turbofan jet engine to analyse the impact of deteriorated components on the overall performance, aerodynamics, aeroelastics, and structural dynamics for the virtual repair process (Schwerdt et al., 2019; Goeing et al., 2020).

In general, the degradation phenomena with impact on the aerodynamic performance of a highly loaded high-pressure compressor and high-pressure turbine in jet engines are, among others, increased tip clearance, changes of airfoil geometry and surface quality (Saravanamuttoo et al., 2001; Kurz et al., 2009). The impact of these effects on the aerodynamics of the individual engine components can be simulated by using RANS simulations (Seehausen et al., 2020). These simulations generate performance maps, which can be utilised in Reduced Order Models (ROM) for the computation of the overall performance (Li et al., 2011; Reitz et al., 2018). Especially during transient manoeuvres, loads can increase significantly (Goeing et al., 2020).

Compared to existing industrial techniques, which are based on experience, this numerical approach yields a scientific method to investigate the impact of deterioration on the overall performance. Thus, economically meaningful decisions can be made by evaluating test cell data of engines in service, using this method. Here, the transient performance of the V2500-A1 engine with miscellaneous and combined deteriorated components is investigated. Hence, RANS simulations of the high-pressure compressor (HPC) and turbine (HPT) are conducted. They include increased surface roughness of the HPC blading's surface and increasing tip clearance of the HPT blades. The results of these simulations are steady-state performances maps. The transient performance is computed with the in-house performance software ASTOR (AircraftEngine Simulation for Transient Operation Research). Common performance tools are based on iterative techniques (Kurzke, 2012) or hybrid numerical/iterative approaches with intercomponent volume methods (Evans et al., 1998; Rahman and Whidborne, 2009). In contrast, ASTOR is based on the Pseudo Bond Graph theory. With the Bond Graph approach, the requirement of graphical programming environments like Simulink is no longer necessary. This is a numerical approach which does not employ iterative techniques and is able to simulate transient performance with higher accuracy, by a reducing simulation speed (Fawke and Saravanamuttoo, 1971; Ganji et al., 1993; Kim et al., 2001).

So far, fast iterative or hybrid numerical/iterative approaches are available and used for a fast calculation in the design process or for real-time simulations in system control. In the maintenance, repair, and overhaul (MRO) industry, a precise prediction of deterioration is of high relevance. In general, the deterioration of single or combined components has a significant effect on the steady and transient performance. Steady performance is used to classify the type and degree of deterioration. However, in jet engines with combined deteriorated components a characterisation of the type of deterioration is more complex. The decision of which component to repair is of economic interest. Subsequently, this investigation maintains that the simulation of transient performance supports this decision significantly.

Therefore, the aerodynamics of the HPC with increasing roughness on blades and HPT with increasing tip clearance are simulated with non-commercial RANS flow solver TRACE. Afterwards, a simplified test procedure is computed with ASTOR to analyse the transient performance of the following four engines: A new engine, an engine with a deteriorated HPC, an engine with deteriorated HPT and an engine with deteriorated HPC and HPT. Different characteristic quantities such as thrust specific fuel consumption (TSFC), temperatures (T) and rotational speed (N_2) are evaluated to determine the type and magnitude of the engine deterioration. Furthermore, transient loads and the surge margin are considered for the deterioration analysis.

Finally, a simplified combined engine model is derived to constitute a relation between the results of engines with single component deterioration to the engine which features multiple deteriorated components. This simplified combined engine should be able to estimate transient and steady performance of a combined deteriorated jet engine without the need to simulate the combined deteriorated jet engine.

Material and methods

This study investigates the V2500-A1 turbofan by International Aero Engines (IAE). The V2500 engines are mounted on the Airbus A320-100. At the beginning, the performance simulation tool ASTOR is explained. Afterwards, the CFD simulations of the HPC and HPT of the V2500-A1 are presented.

Performance simulation

The influence of deteriorated components on the overall performance of a jet engine is simulated with the IFAS in-house performance software tool ASTOR. Therefore, all equations of motion and further ordinary differential

equations for heat flow or spool speed are solved using a Runge Kutta third order algorithm. The pseudo Bond Graph is shown in Figure 1. Here, efforts e (e.g. pressure p , temperature T or torque τ) and flows f (e.g. mass flow \dot{m} , energy flow E , heat flow \dot{Q} or rotational speed N) of the physical domains represented within a jet engine are laid out. The 0- and 1- junctions are applied to connect these efforts e and flows f of the miscellaneous domains. In the gas path, the conservation of momentum is solved at the 1- junction and the conservation of energy and mass, including heat transfer and secondary air flow, at the 0- junction. Therefore, gas effects, which are based on inertia (I_G (see (Lueck et al., 2020))) and capacity (C , C_T and C_W) (mass storage and dynamic volumes), are directly included in the system of differential equations.

Performance maps contain the boundary conditions for the miscellaneous domains. The sections of choked flow in compressor and turbine performance maps constitute a challenge for map interpolation since the reduced mass flow does not increase anymore while pressure ratio change. In order to enable an algorithmic solution of the proposed interpolation technique (Goeing et al., 2019), infinitesimal increments of reduced mass flow \dot{m}_{corr} are added to enforce a strictly monotonous increase of mass flow. Therefore, ambiguities are removed where previously multiple pressure ratios were assigned to a single mass flow value. Moreover, the Piecewise Cubic Hermite Interpolating Polynomial (PCHIP) (Fritsch and Carlson, 1980) or Akima (Akima, 1970) algorithm and a linear scaled interpolation is used for a high resolution between and on the characteristic curves.

Apart from the performance maps of the miscellaneous components, characteristic lengths, cross sectional areas as well as material information are required for the equations. Scaled performance maps of the fan and booster are used (Wolters et al., 2016; Vieweg et al., 2017) and a simulated low-pressure turbine (LPT) map was calculated in (Ulrich, 2019). Next, based on the IFAS inhouse V2500-A1 engine a full CAD-model was designed to determine the characteristic lengths (see background of Figure 1). Therefore, the fan, HPC, HPT and LPT blades are weighed to determinate the mass. The weight of the booster blades, the two spools and discs are approximated and based on technical sketches. Mostly, titanium and nickel alloys are used as material for these components. The resulting moment of inertia of the LP-system is $57 \text{ kg}\cdot\text{m}^2$ and that of the HP-system $11 \text{ kg}\cdot\text{m}^2$.

CFD methods

The CFD simulations of the HPC and HPT are performed using the non-commercial flow solver TRACE of the German Aerospace Center (DLR) in version 9.0 and 9.1 (Nuernberger, 2004; Franke et al., 2005; Kugeler et al., 2008). Based on a finite-volume method with structured multi-block meshes, the three-dimensional Favre-averaged Navier-Stokes equations are solved. The discretisation of the convective fluxes is performed by

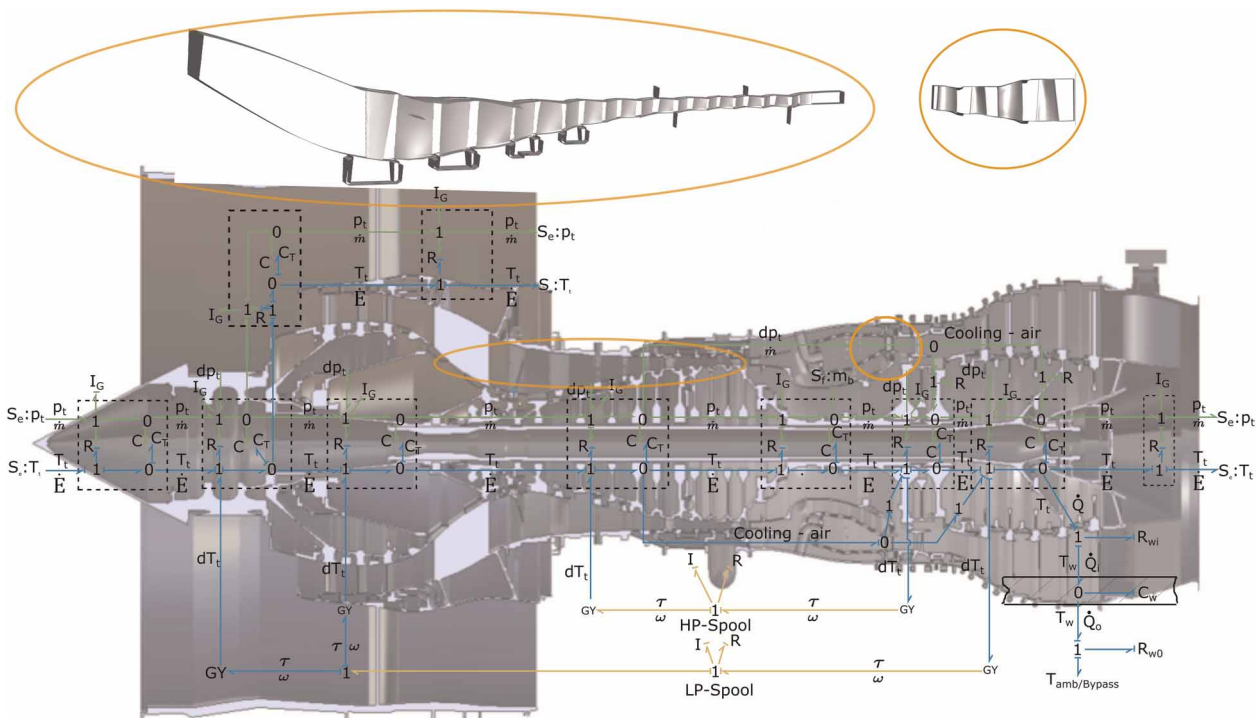


Figure 1. CAD model and Pseudo Bond Graph of the V2500-A1. Expansion of the HPC/T (left/right).

Roe's second-order upwind scheme, while the diffusive fluxes are solved by a 2nd order central differencing scheme. An automated Python-script is used to generate the performance maps required by ASTOR. The script varies, in steps, the static outlet pressure of the HPC simulations and total inlet pressure of the HPT simulations. The inlet and outlet boundary conditions are derived from full performance synthesis calculations. Different rotational speeds are considered, and the meshing was performed using Numeca Autogrid software. The numerical setups are presented in Table 1. A mesh convergence study of the HPC setup resulting in a mesh with approximately 26 million cells and a validation of the simulated HPC performance maps are presented in (Reitz et al., 2018). In addition, a mesh convergence study was carried out for HPT, which results in a Grid Convergence Index (Roache, 1993) of 0.0084 and the asymptotic character of the grid convergence was confirmed with 1.0058. Based on Sridhar (Sridhar et al., 2011), the Menter SST turbulence model (Menter, 1994) is applied for these simulations. The multimode model is used for transition, which is validated particularly for turbomachinery applications (Kožulović, 2007).

The CFD results are evaluated in terms of the corrected mass flow \dot{m}_{corr} :

$$\dot{m}_{\text{corr}} = \dot{m}_{\text{in}} \cdot \frac{101325 \text{ Pa}}{P_{\text{in}}} \cdot \frac{\sqrt{T_{\text{in}}}}{288.15 \text{ K}} \quad (1)$$

polytropic efficiency η_{pol} (Dixon and Hall, 2013):

$$\eta_{\text{pol}} = \frac{\kappa - 1}{\kappa} \cdot \frac{\log(\pi_{tt})}{\log(\tau_{tt})} \quad (2)$$

total temperature ratio τ_{tt} :

$$\tau_{tt} = \frac{T_{t,\text{out}}}{T_{t,\text{in}}} \quad (3)$$

total pressure ratio π_{tt} :

$$\pi_{tt} = \frac{P_{t,\text{out}}}{P_{t,\text{in}}} \quad (4)$$

HPC surface roughness

The operation of an aircraft engine causes several different deterioration modes acting on the engine performance. One significant factor when focusing on the performance reduction of an HPC is described by surface roughness (Seehausen et al., 2020). Based on environmental factors such as aerosols, dust, and other particles, blade's

Table 1. CFD setup of the HPC and HPT.

Settings	HPC	HPT
Analysis type	Steady state	Steady state
Walls	No slip walls	No slip walls
Interface between rows	Mixing plane	Mixing plane
Turbulence model	Wilcox $k - \omega$ (Wilcox, 1988)	Menter SST (Menter, 1994)
Transition model	Off/ fully turbulent	Multimode (Kožulović, 2007)
Rotational speeds N_2 in rpm	11,876–14,391	9,640–13,972

surface roughness is increased, resulting in performance losses (Tarabrin et al., 1998; Morini et al., 2009; Bons, 2010; Wensky et al., 2010). Gilge et al. optically measured the blade surfaces of HPCs which had completed 20,000 cycles (Gilge et al., 2019a, b). Additionally, the equivalent sand-grain roughness k_s is calculated using the correlation of (Bons, 2005) in conjunction with the shape and density parameter of (Sigal and Danberg, 1990). The k_s values calculated were used by (Seehausen et al., 2020) to study the multistage effect of surface roughness. Based on previous studies, (Seehausen et al., 2020) could extrapolate the measurements of (Gilge et al., 2019a, b) to all blades of the HPC. Figure 2 presents the extrapolated average roughness height across the stages on blades and vanes, on both suction and pressure side. The surface roughness significantly decreases across the first half of the HPC, caused by deposits and particle impacts on the suction side. On the pressure side, a more homogeneous roughness distribution is formed. To illustrate the complexity of the surfaces examined, examples of characteristic surface structures depending on the position in the HPC are shown in Figure 2.

In (Goeing et al., 2020), the effect of HPC surface roughness on the transient engine performance was extensively investigated in ASTOR. To model the transient manoeuvre in ASTOR, performance maps at different rotational speeds and roughness levels are calculated using numerical solutions from TRACE. Following which, the performance maps are scaled using a method described by (Li et al., 2011) which results in lower computational effort. The individual scaling factors indicate a dependency between the Reynolds-number and the roughness effect, which is consistent with the findings of (Nikuradse, 1933; Moody, 1944). In the left plots of Figure 3, the HPC performance maps used in this study are illustrated. The green lines represent the map of the smooth blades and vanes, while the black lines correspond to scaled maps of average roughness height after 20,000 cycles in service.

Surface roughness reduces the mass flow due to thicker boundary layers. This comes along with a decreased efficiency and increased pressure losses. At low rotational speeds, the effect of surface roughness increases due to smaller Reynolds numbers.

Reitz (Reitz et al., 2018) performed a scaling of the HPC performance map with a doubled tip gap size. As shown by (Seehausen et al., 2020), the overall effect on the performance is larger for surface roughness than for tip gaps. In contrast to surface roughness, doubled tip gaps mainly affect the polytropic efficiency and not the pressure rise. A CFD study by (Reitz and Friedrichs, 2018) on the effect of modified geometries in the front and rear stages, caused by deterioration, revealed that the performance could be increased by local geometry changes. The intensity of the effect strongly depends on the geometrical parameter modified and varies with the stage (Lange et al., 2012). Regardless of the deterioration type, i.e. surface roughness or geometrical deterioration, the performance is predominantly affected by the front stages resulting in multistage effects.

HPT tip clearance

HPT blades and vanes are exposed to high thermal and mechanical loads due to high gas temperatures and rotational speeds. This causes a range of different deterioration types, an increased blade tip gap being one of them. Typically, the gaps between the turbine blade tips and the shroud are designed to be as small as possible. As described by (Denton, 1993), the secondary flow in the tip gap contributes significantly to the losses in the turbine. Bindon showed that the losses increase with increasing radial gap (Bindon, 1989). To investigate the effect of the increased radial gap on the overall performance, the CFD simulations of the V2500-A1's HPT are performed.

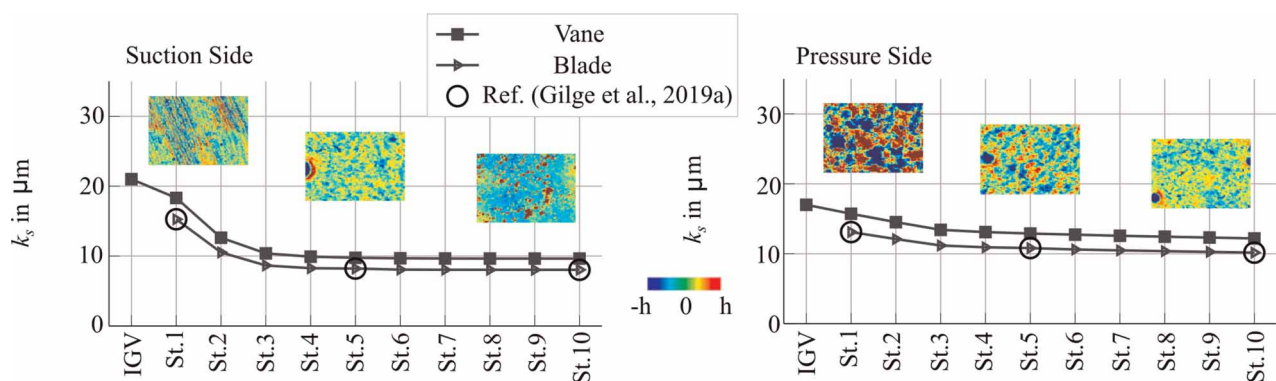


Figure 2. Roughness distribution across the stages of the HPC after 20,000 cycles in service and examples of measured surfaces (Gilge et al., 2019a).

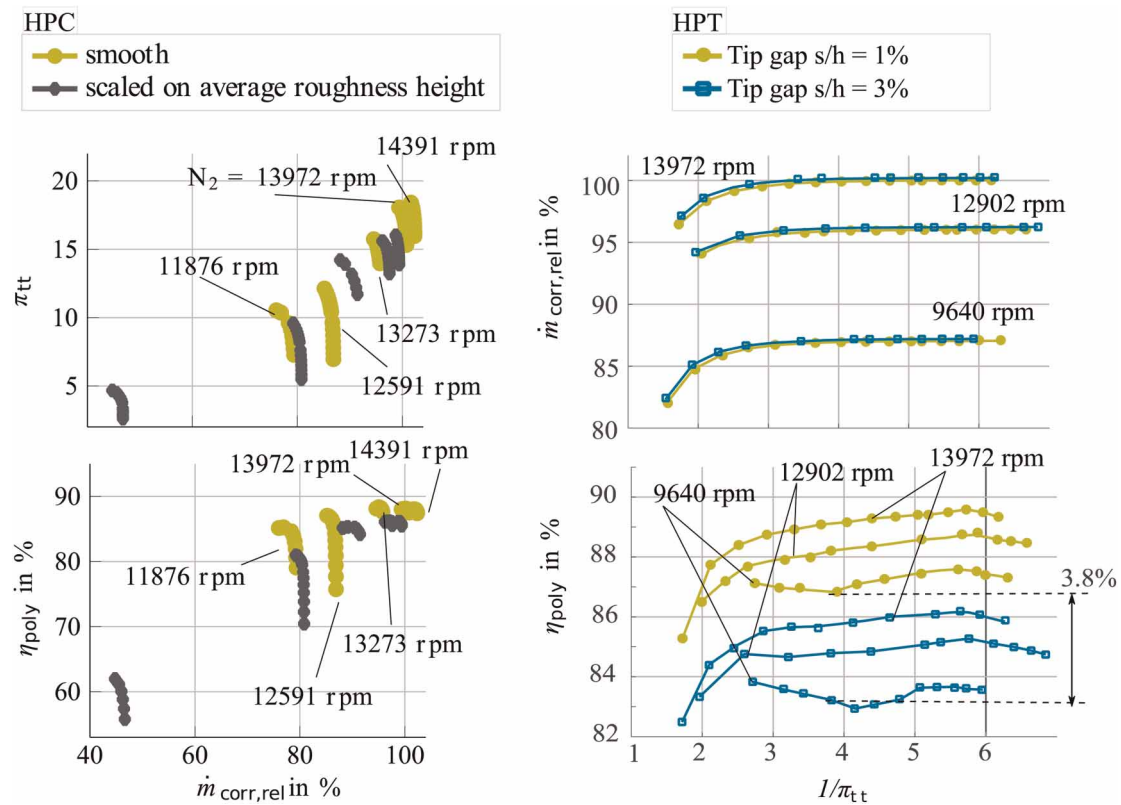


Figure 3. CFD performance maps. Left: Performance map of the HPC with smooth blades and vanes at different rotational speeds compared with the scaled map of average roughness height. Top: Pressure ratio π_{tt} over mass flow \dot{m} . Bottom: Polytropic efficiency η_{pol} over mass flow \dot{m} . Right: Turbine performance maps with different tip gaps. Top: Mass flow \dot{m} over pressure ratio $1/\pi_{tt}$. Bottom: Polytropic efficiency η_{pol} over pressure ratio $1/\pi_{tt}$.

The V2500-A1 HPT consists of two stages and in this study the blade tip gaps of both stages are varied. The variation is set as a ratio of radial gap s and blade height h . Accordingly, two meshes with different s/h ratios are created. A ratio of $s/h = 1\%$ is used as a reference and the increased tip gap is represented by $s/h = 3\%$. Table 2 summarises the meshing setup for tip gaps.

Results are evaluated in terms of corrected mass flow \dot{m}_{corr} and polytropic efficiency η_{pol} as a function of the total pressure ratio $1/\pi_{tt}$. The resulting HPT performance maps are shown in the right diagrams of Figure 3.

The lower plot of the right diagrams in Figure 3 shows the influence of the increased gap (blue lines) on the polytropic efficiency. The higher radial tip gap decreases polytropic efficiency by up to 3.8% across all speed lines, which corresponds to earlier studies (Hourmouziadis and Albrecht, 1987). This is caused by increased secondary flow losses in the tip gap. Hence, a negative effect of the increased tip gap on the overall HPT performance can be observed. The influence on the corrected mass flow is not as explicit and decreases by only 0.06%–0.35%

Table 2. Tip gap meshing.

Stage	1st		2nd	
	1%	3%	1%	3%
s/h	1%	3%	1%	3%
s in mm	0.47	1.40	0.66	1.98
Radial gap nodes	25	25	25	25

Results and discussion

In this chapter, the overall performance of the miscellaneous jet engines is presented and discussed in more detail. The performance is simulated for a simplified test manoeuvre derived from the pass-off test procedure of the V2500 engine. This test procedure considers 4 different thrust levels (Band A - 105 kN, Band B - 95 kN, Band C - 80 kN and Band D - 30 kN) and a slam acceleration between the Band D and A at the beginning. In addition, a slam deceleration is simulated between each adjoining thrust level. Furthermore, a linear fuel flow signal between the thrust levels is applied. The full manoeuvre ends after 30 s.

The following miscellaneous jet engines are investigated:

1. New engine Θ_1
2. Engine with deteriorated HPC Θ_2
3. Engine with deteriorated HPT Θ_3
4. Engine with deteriorated HPC and HPT Θ_4
5. Simplified combined (sim. com.) engine Θ_5

The combined jet engine Θ_4 is compared to a simplified combined engine Θ_5 . This simplified combined engine is a relation between the product of both engines with a single deteriorated domain and the new engine as follows:

$$\Theta_5 = \frac{\Theta_2 \cdot \Theta_3}{\Theta_1} \quad (5)$$

Steady and transient performance

In this section, characteristic quantities of the test procedure are analysed. They are used to describe the degree of engine deterioration and give an estimation about the component that is subject to deterioration. In the beginning, the transient performance of the engines is represented by quantities which can be measured at the V2500 during a pass off test after a shop visit. Afterwards, the impact on the HPC stability margin is discussed. In the following diagrams, the new engine Θ_1 is represented in green with crosses, the engine with a high level of blade roughness in the HPC Θ_2 in black with rightward-pointing triangles, the engine with increased tip gaps Θ_3 in blue with left-pointing triangles, the combined engine Θ_4 in red with plus signs and the simplified combined engine Θ_5 in yellow with squares.

Thrust specific fuel consumption (TSFC)

In the upper left diagram of [Figure 4](#) the thrust specific fuel consumption (TSFC) is shown over the time t for all engines. In general, the full TSFC range is between 6.3–15.5 g/(kN·s). During the slam acceleration, the TSFCs have overshoots, due to the spool's inertia and the resulting attenuated mass flow. The same effects are responsible for the peaks during decelerations. It is recognisable, that the TSFC of the new engine is consistently the lowest. The mean TSFC of engine Θ_2 is 5.1% higher and Θ_3 is 4.9% higher compared to Θ_1 with changing signs at Band B. Moreover, Θ_2 has got an increased sensitivity towards transient operation, indicated by the higher peaks. The combined deteriorated engine Θ_4 constantly shows the highest TSFC at each thrust level throughout the entire performance simulation. The predicted TSFC is 10.2% higher compared to the new engine. Therefore, an engine with combined degradation domains, thus a higher degree of overall deterioration, requires more fuel flow to achieve the same thrust levels. Additionally, the simplified combined engine Θ_5 shows an accurate prediction in Band C and D.

Exhaust gas temperature (EGT)

Like the TSFC, the exhaust gas temperature (EGT) downstream of the low-pressure turbine is an important identifier for the degree of deterioration. The course of the EGT is plotted over time t in the diagram on the bottom left of [Figure 4](#). Furthermore, the steady state EGTs are represented with dots for each thrust level for the new engine. In these curves, different transient effects are visible. During acceleration and deceleration, the impact of in-/decreasing fuel to air ratio is visible due to the shaft/gas inertia. In the constant fuel flow regions, temperature is increasing slowly due to the heat flow from gas to material. Subsequently, the steady performance is not reached after the 10 s duration of each Band. Like the TSFC, the highest EGT is attained by Θ_4 . The mean deviation from the new engine Θ_1 is 12.5% (12.9% for the simplified combined engine Θ_5). The deterioration of the HPC as well as the HPT results in a higher EGT. Both engines Θ_2 and Θ_3 are at a similar EGT

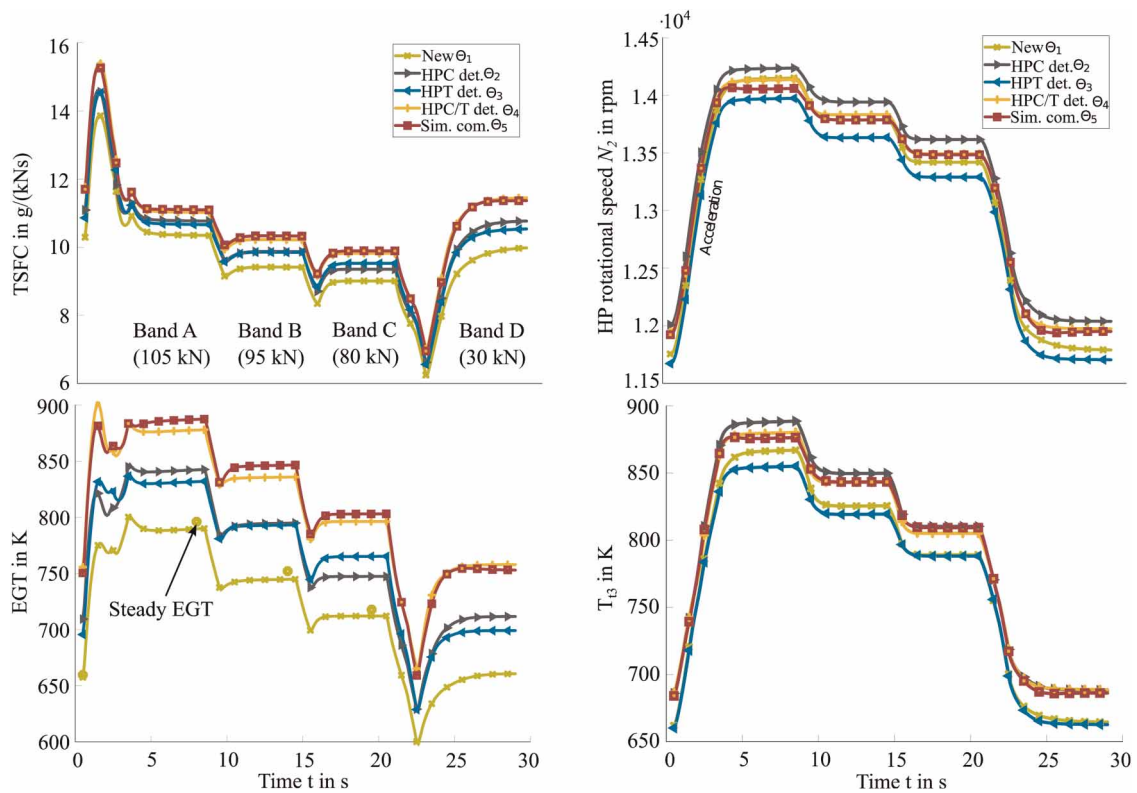


Figure 4. Left: Identification of the degree of deterioration of the 5 engines. Upper left: Thrust specific fuel consumption (TSFC) over the time t during the pass off test. Bottom left: Exhaust gas temperature (EGT) over the time t . The dots represent the EGT of the steady operating points of the new engine. Right: Identification of the cause of deterioration. Upper right: High-pressure rotational speed (N_2) over the time t during the pass off test. On the bottom right: Temperature downstream of the HPC (T_{t3}) over the time t during the pass off test.

level with changing sign in Band B. The mean EGT is up to 6.3% higher compared to the new engine. Furthermore, the transient peaks are more pronounced in Θ_2 and Θ_3 . These peaks increase even more for the combined engine Θ_5 .

The TSFC and EGT are feasible to determine the degree of deterioration. Obviously, the combined engine has the highest level, but these identifiers are not sufficient to grade the single deteriorated engines.

HP rotational speed N_2

In the upper right diagram of Figure 4 the HP system’s rotational speed N_2 is plotted during the test. In contrast to TSFC and EGT, the order of the spool speed levels does not correspond to the level of deterioration. Here, the highest rotational speed is detected at engine Θ_2 . Hence, this engine achieves the target thrust levels with a higher speed compared to the new engine (1.4% on average).

In addition, engine Θ_3 requires a significantly lower spool speed during the manoeuvre (–1% on average). In contrast to engines Θ_2 and Θ_3 , engine Θ_4 is within the same range as the new engine. Only at Band D Θ_3 is close to the new engine while, Θ_4 is close to Θ_2 . In general, the pseudo engine Θ_5 is approximately coincident to Θ_4 . The same deviations are visible during Band A and Band D for these two engines.

Temperature T_{t3}

In contrast to p_{t5} and LP rotational speed N_1 , the temperature T_{t3} shows a did not understand the meaning. This temperature is measured in the V2500 for burner flame out protection. Other engines (e.g. CF34) are not equipped to measure this value. The total temperature T_{t3} is shown on the bottom right of diagram of Figure 4. Like the rotational speed, engine Θ_2 has the highest T_{t3} value at all thrust levels. Basically, the temperature is up to 2.9% higher compared to Θ_1 . On the other hand, a deteriorated HPT of Θ_3 results in a lower temperature.

The mean deviation from the new engine is -0.6% . In contrast to the spool speed, Θ_4 is higher than the new engine (2.3% on average). The simplified combined engine Θ_5 approximates coincides with Θ_4 .

Surge margin SM

The interaction between deterioration and stability of the system is investigated using the HPC surge margin. The change in HPC surge margin compared to the steady state operating line is analysed over rotational speeds N_2 during acceleration (Band D to Band A) in the right diagrams of Figure 5.

The definition of the surge margin SM is given in Equation 6:

$$SM = \frac{\pi_{SL}}{\pi_{OP}} \cdot \frac{\dot{m}_{OP}}{\dot{m}_{SL}} - 1 \text{ with } \dot{m} = \text{const.} \tag{6}$$

The relative deviations between transient and steady operating line are calculated with

$$\Delta SM_{rel. \text{ steady}} = \frac{SM_{\text{transient}} - SM_{\text{steady}}}{SM_{\text{steady}}} \tag{7}$$

In the right diagram of Figure 5, the SM of the transient operating line (OL) is between 0.52 and 0.22 for the new engine. Compared to the steady state OL, the SM decreases up to -21% (see left diagram of Figure 5). A significant contrast to Θ_1 is visible in the SM of Θ_2 . This SM is between 0.31 and 0.07. Moreover, the deviation from the steady operating line has a maximum of -35% . The stability of Θ_3 is similar to Θ_1 . However, an offset is present and the SM of the transient OL is between 0.50 and 0.21 with a maximum of -22% to the steady state OL. Furthermore, the OL moves towards lower rotational speeds.

The impact of combined HPC/T deterioration is shown by Θ_4 . The SM has the largest offset to the new engine and is between 0.3 and 0.08. The max. deviation to the state steady OL is like Θ_2 with -37% . The simplified combined engine Θ_5 corresponds to Θ_4 . A significant difference in the performance between the engine Θ_2 and Θ_3 is visible. Therefore, the highest deterioration is found in engine Θ_4 , followed by engine Θ_2 .

Summary/Explanation

In Figure 4 different identifiers for the overall degree of engine deterioration as well as components affected by deterioration have been analysed. In general, two effects are responsible for the performance degradation. First, the reduced efficiency η_{pol} of HPT and HPC is comparable to a reduction of nozzle cross sectional area and a shift of the HPC OL above the OL of a new engine (throttle effect). Second, the deteriorated HPC changes the shape of the HPC performance map and the position of the stability line moves towards the OL (shift effect) (see upper left diagram of Figure 3).

The HPC of Θ_2 is not able to provide enough pressure for the energy recovery in the HPT (shift effect). Hence, the fuel flow increases to achieve the same thrust level, which results in a higher EGT. Subsequently, the

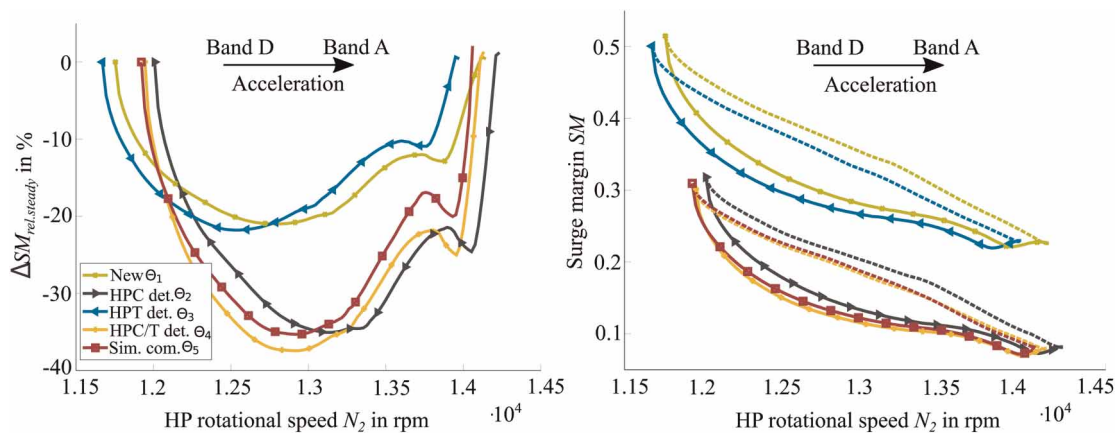


Figure 5. System stability during the acceleration between 0 s and 8 s. Right: Surge margin of operating line in HPC performance map over the spool speed N_2 of the HPC. Transient operating line in solid lines and with marker, steady in dashed lines. Left: Relative deviations between transient and steady HPC operating line.

rotational speed increases the pressure level which delivers enough pressure (with the combination of fuel flow). Furthermore, a reduced HPC η_{pol} increases the compressor exit temperature T_{t3} (see Equation 2).

The reduced HPT efficiency (see bottom right diagram of Figure 3) results in a decreased energy output from the turbine with a smaller pressure ratio $1/\pi_{tt}$. This results in a smaller compressor pressure ratio π_{tt} and mass flow (throttle effect). Consequently, the rotational speed decreases and more fuel flow is necessary to achieve the same thrust level (EGT increases).

The combination of both degradations increases the EGT significantly compared to the other engines. However, the performance impact of deteriorated HPT dampens the increasing temperature T_{t3} and spool speed N_2 of the responsible deteriorated HPC, compared to the engine Θ_2 . Therefore, both curves move in the direction of the new engine performance.

In the next step of this analysis, the impact of transient loads and system stability is investigated. Especially during the acceleration, an increasing EGT peak occurs due to the system's inertia (see Figure 4). The reduced mass flow has an impact on the fuel to air ratio and therefore on the transient loads. Hence, the reduced mass flow $\Delta\dot{m}$ decreases for both degradations, due to the shifted operating lines (throttle effect) and the shape of the characteristic curves.

Furthermore, both effects have a significant impact on the surge margin. The degree of HPC/T deterioration are at the same level (see TSFC and EGT), but the SM of Θ_2 is significantly lower than that of Θ_3 . Therefore, the second effect (shift effect) has a higher influence on the system stability compared to the throttle effect.

Finally, the simplified combined engine model Θ_5 can be used to represent this performance and is close to the values of Θ_4 .

The shift and throttle effect influence the engine performance in different ways. However, the modified compressor and turbine aerodynamics with further deteriorations such as a reduced leading/trailing edge, max. thickness and the resulting stagger angle are investigated in several studies (Scharfenstein et al., 2013; Reitz et al., 2014; Ernst et al., 2016). These results exhibit that the positions of the characteristic curve (mass flow, pressure ratio and efficiency) are qualitatively and quantitatively dependents on the type of deterioration. Based on the results of engine Θ_4 , it can be concluded that combined degradation in one turbomachine increases the deterioration of engine performance and stability, but also dampen it.

Conclusions and outlook

In this paper, the impact of combined deteriorated components in a turbofan jet engine has been investigated. The aerodynamics as well as the performance of the HPC and HPT of the V2500-A1 engine were simulated using RANS methods. The influence of degradation represented by increasing roughness in the HPC and tip clearance in the HPT on the performance maps was computed. The derived performance maps were used to simulate the overall performance of the jet engine. A simplified test procedure was used to analyse the impact of the deterioration on the steady and transient performance at different thrust levels and in transient load cases with ASTOR. The characteristic effects of the degradation on the performance can be summarised as follows:

1. TSFC and EGT can be used to identify the degree of deterioration
2. T_{t3} and N_2 can be used to identify the component affected by deterioration.
3. HPC surge margin and the deviation between transient and steady operating line have a significant difference for HPT and HPC deterioration.
4. Transient loads increase significantly for a combined deteriorated engine.
5. Steady and transient performance of a combined deterioration jet engine can be approximated by the coupling of the single deterioration jet engines.

A reduction of the HPC's blade roughness and a recovery of the HPT tip clearance in a high bypass jet engine improves the engine performance significantly. Both isolated and combined degradation effects increase the specific fuel consumption and operating costs during the full manoeuvre. However, the recovery of the HPT in a combined deteriorated engine has a subordinate influence on the surge margin in the HPC. Nevertheless, transient loads can be reduced significantly by recovering only one domain. These results can be used to classify deterioration by evaluating steady and transient test cell data, improve safety limits and extend life cycles. Finally, the relevance to consider deterioration of engine components in transient operations was shown.

This investigation will be extended by the impact of deteriorated combustion chambers. Moreover, an individual pass off test of the instrumented IFAS in-house V2500-A1 jet engine with combustion chamber modifications will be performed and simulated with ASTOR. Furthermore, the impact of combined deterioration effects in one turbomachine on the overall transient performance and stability should be investigated.

Nomenclature

C	Capacity element
C_T	Thermodynamic accumulator
C_{TW}	Capacity element for heat flow
c_p	Specific heat coefficient
ΔT	Temperature rise
Δp	Pressure rise
e	Effort
\dot{E}	Energy flow
f	Flow
h	Blade height
k	Turbulent kinetic energy, heat capacity ratio
k_s	Sand roughness
I	Inertia element
J	Moment of inertia
\dot{m}	Mass flow
N	Rotational speed
p	Pressure
π	Pressure ratio
\dot{Q}	Heat flow
red	Reduced value
R	Resistor
s	Gap
t, tt	Time, total, total to total
T	Temperature
η	Efficiency
Θ	Engine
τ	Torque, temperature ratio
ω	Specific dissipation
ASTOR	AircraftEngine Simulation for Transient Operation Research
CAD	Computer-Aided Design
CFD	Computational Fluid Dynamics
Corr	Corrected
CRC	Collaborative Research Centre
DFG	German Research Foundation
DLR	German Aerospace Center
EGT	Exhaust Gas Temperature
IAE	International Aero Engines
IFAS	Institute of Jet Propulsion and Turbomachinery
HP	High-pressure
HPC	High-pressure compressor
HPT	High-pressure turbine
LP	Low-pressure
LPC	Low-pressure compressor
LPT	Low-pressure turbine
MRO	Maintenance, repair and overhaul
PCHIP	Piecewise Cubic Hermite Interpolating Polynomial
Pol	Polytropic
RANS	Reynolds-Averaged Navier-Stokes
ROM	Reduced Order Model
OL	Operating line
OP	Operating point
Sim. Com.	Simplified combined
SL	Surge line
SM	Surge Margin

SST Shear Stress Transport
 TSFC Thrust specific fuel consumption

Acknowledgments

The present work has been carried out in the subprojects D6, B3, A3 within the Collaborative Research Center (CRC) 871 “Regeneration of Complex Capital Goods” which is funded by the Deutsche Forschungsgemeinschaft (DFG, German Research Foundation) – SFB 871/3–119193472. The authors would like to thank the DFG for the support. Moreover, the authors would like to acknowledge the substantial contribution of the DLR Institute of Propulsion Technology and MTU Aero Engines AG for providing TRACE.

Funding sources

Deutsche Forschungsgemeinschaft (DFG, German Research Foundation) – SFB 871/3 – 119193472.

Competing interests

Jan Göing declares that he has no conflict of interest. Hendrik Seehausen declares that he has no conflict of interest. Vladislav Pak declares that he has no conflict of interest. Sebastian Lück declares that he has no conflict of interest. Joerg R. Seume declares that he has no conflict of interest. Jens Friedrichs declares that he has no conflict of interest.

References

- Akima H. (1970). A new method of interpolation and smooth curve fitting based on local procedures. *Journal of the ACM (JACM)*. 17 (4): 589–602. <https://doi.org/10.1145/321607.321609>
- Bindon J. P. (1989). The measurement and formation of tip clearance loss. *Journal of Turbomachinery*. 111 (3): 257–263. <https://doi.org/10.1115/1.3262264>
- Bons J. (2005). A critical assessment of reynolds analogy for turbine flows. *Journal of Heat Transfer*. 127 (5): 472–485. <https://doi.org/10.1115/1.1861919>
- Bons J. P. (2010). A review of surface roughness effects in gas turbines. *Journal of Turbomachinery* (132): 21004. <https://doi.org/10.1115/1.3066315>
- Denkena B., Nyhuis P., Bergmann B., Nuebel N., and Lucht T. (2019). Towards an autonomous maintenance, repair and overhaul process: Exemplary holistic data management approach for the regeneration of aero-engine blades. *Procedia Manufacturing*. 40: 77–82. <https://doi.org/10.1016/j.promfg.2020.02.014>
- Denton J. D. (1993.) *Loss Mechanisms in Turbomachines*. Cincinnati: American Society of Mechanical Engineers.
- Dixon S. L. and Hall C. (2013). *Fluid Mechanics and Thermodynamics of Turbomachinery*. Amsterdam: Butterworth-Heinemann.
- Ernst B., Seume J. R., and Herbst F. (2016). Probabilistic cfd-analysis of regeneration-induced geometry variances in a low-pressure turbine. *52nd AIAA/SAE/ASEE Joint Propulsion Conference*, p. 4555. <https://doi.org/10.2514/6.2016-4555>
- Evans A., Follen G., Naiman C., and Lopez I. (1998). Numerical propulsion system simulation’s national cycle program. *34th AIAA/ASME/SAE/ASEE Joint Propulsion Conference and Exhibit*, p. 3113. <https://doi.org/10.2514/6.1998-3113>
- Fawke A. J. and Saravanamuttoo H. I. H. (1971). Digital computer methods for prediction of gas turbine dynamic response. *SAE Transactions*. 80: 1805–1813.
- Franke M., Kuegeler E., and Nuernberger D. (2005). Das DLR-Verfahren TRACE: Moderne Simulationstechniken fuer Turbomaschinenstroemungen. DGLR Congress.
- Fritsch F. N. and Carlson R. E. (1980). Monotone piecewise cubic interpolation. *SIAM Journal on Numerical Analysis*. 17 (2): 238–246. <https://doi.org/10.1137/0717021>
- Ganji A. R., Khadem M., and Khandani S. M. H. (1993). Transient dynamics of gas turbine engines. *ASME 1993 International Gas Turbine and Aeroengine Congress and Exposition*, p. V03CT17A014. <https://doi.org/10.1115/93-GT-353>
- Gilge P., Kellersmann A., Friedrichs J., and Seume J. R. (2019a). Surface roughness of real operationally used compressor blade and blisk. *Proceedings of the Institution of Mechanical Engineers, Part G: Journal of Aerospace Engineering*. 233 (14): 5321–5330. <https://doi.org/10.1177/0954410019843438>.
- Gilge P., Kellersmann A., Kurth S., Herbst F., Friedrichs J., and Seume J. R. (2019b). Dataset: Surface Roughness of Real Operationally Used Compressor Blade and Blisk. *Research Data Repository of the Leibniz University of Hannover*. Available at: <https://doi.org/10.25835/0084372>
- Goeing J., Lueck S., Bode C., and Friedrichs J. (2019). Simulation of the impact of a deteriorated high-pressure compressor on the performance of a turbofan engine using a pseudo bond graph modeling approach. *Global Power and Propulsion Society*. <https://doi.org/10.33737/gpps19-bj-160>
- Goeing J., Seehausen H., Bode C., Herbst F., Seume J. R., and Friedrichs J. (2020). Performance simulation of roughness induced module variations of a jet propulsion by using pseudo bond graph theory. *ASME Turbo Expo 2019: Turbomachinery Technical Conference and Exposition*.
- Hourmouziadis J. and Albrecht G. (1987). An integrated aero/mechanical performance approach to high technology turbine design. *Advisory group for aerospace research & development, Paris*.

- Kim J. H., Song T. W., Kim T. S., and Ro S. T. (2001). Model development and simulation of transient behavior of heavy duty gas turbines. *Journal of Engineering for Gas Turbines and Power*. 123 (3): 589–594. <https://doi.org/10.1115/1.1370973>
- Kožulović D. (2007). Modellierung des Grenzschichtumschlags bei Turbomaschinenstroemungen unter Beruecksichtigung mehrerer Umschlagsarten. PhD, Ruhr-Universitaet Bochum.
- Kugeler E., Nuernberger D., Weber A., and Engel K. (2008). Influence of blade fillets on the performance of a 15 stage gas turbine compressor. *ASME Turbo Expo 2008: Power for Land, Sea, and Air*, pp. 415–424. <https://doi.org/10.1115/GT2008-50748>
- Kurz R., Brun K., and Wollie M. (2009). Degradation effects on industrial gas turbines. *Journal of engineering for gas turbines and power*. 131 (6). <https://doi.org/10.1115/1.3097135>
- Kurzke J. (2012). GasTurb 12: A program to calculate design and off-design performance of gas turbines. User manual.
- Lange A., Voigt M., Vogeler K., Schrapp H., and Johann E. (2012). Impact of manufacturing variability on multistage high-pressure compressor performance. *Journal of Engineering for Gas Turbines and Power*. 134 (11). <https://doi.org/10.1115/1.4007167>
- Li Y. G., Ghafir M. F., Wang L., Singh R., Huang K., and Feng X. (2011). Nonlinear multiple points gas turbine off-design performance adaptation using a genetic algorithm. *ASME Journal of Engineering for Gas Turbines and Powe*. 133 (7): 071701. <https://doi.org/10.1115/1.4002620>
- Lueck S., Goeing J., Bode C., and Friedrichs J. (2020). Pseudo Bond Graph System Modelling Of Electric Air Compressors With Energy Recovery For Fuel Cell Applications. *ASME Turbo Expo 2019: Turbomachinery Technical Conference and Exposition*.
- Menter F. R. (1994). Two-equation eddy-viscosity turbulence models for engineering applications. *AIAA Journal*. 32 (8): 1598–1605. <https://doi.org/10.2514/3.12149>
- Moody L. (1944). Friction factor for pipe flow. *Transactions of the ASME*. 66: 671–684.
- Morini M., Pinelli M., Spina P. R., and Venturini M. (2009). CFD simulation of fouling on axial compressor stages. *ASME Turbo Expo 2009: Power for Land, Sea, and Air*, pp. 331–342. <https://doi.org/10.1115/GT2009-59025>
- Nikuradse J. (1933). Law of Flows in Rough Pipes. *NACA Technical Memorandum 1292*.
- Nuernberger D. (2004). Implizite Zeitintegration fuer die Simulation von Turbomaschinenstroemungen. PhD, Ruhr-Universitaet Bochum.
- Rahman N. U. and Whidborne J. F. (2009). Real-time transient three spool turbofan engine simulation: A hybrid approach. *Journal of Engineering for Gas Turbines and Power*. 131 (5). <https://doi.org/10.1115/1.3079611>
- Reitz G. and Friedrichs J. (2018). Impact of front-and rear-stage high pressure compressor deterioration on jet engine performance. *International Journal of Turbomachinery, Propulsion and Power*. 3 (2): 15. <https://doi.org/10.3390/ijtp3020015>
- Reitz G., Friedrichs J., Marx J., and Stading J. (2014). Performance Analysis of Deteriorated High Pressure Compressor Blades. *Volume 2A: Turbomachinery*, p. V02AT37A014. <https://doi.org/10.1115/GT2014-25544>
- Reitz G., Kellersmann A., and Friedrichs J. (2018). Full High Pressure Compressor Investigations to Determine Aerodynamic Changes due to Deterioration. *ASME Turbo Expo 2018: Turbomachinery Technical Conference and Exposition*, p. V02AT39A035–V02AT39A035. <https://doi.org/10.1115/GT2018-76644>
- Roache P. J. (1993). A method for uniform reporting of grid refinement studies. *ASME-PUBLICATIONS-FED*. 158: 109.
- Saravanamuttoo H. I. H., Rogers G. F. C., and Cohen H. (2001.) *Gas Turbine Theory*. Essex: Pearson Education.
- Scharfenstein J., Heinze K., Voigt M., Vogeler K., and Meyer M. (2013). Probabilistic CFD analysis of high pressure turbine blades considering real geometric effects. *Turbo Expo: Power for Land, Sea, and Air*, p. V06BT43A005. <https://doi.org/10.1115/GT2013-94161>
- Schwerdt L., Berger R., Panning-von Scheidt L., Gebhardt C. G., Wallaschek J., and Rolfes R. (2019). Probabilistic Study of Blend Repairs on an Axial Compressor Blisk using the Subset of Nominal Modes Method. *Proc. IGTC Int. Gas Turbine Congress*.
- Seehausen H., Gilge P., Kellersmann A., Friedrichs J., and Herbst F. (2020). Numerical Study of Stage Roughness Variations in a High Pressure Compressor. *International Journal of Gas Turbine. Propulsion and Power Systems* . 11 (3): 16–25.
- Sigal A. and Danberg J. E. (1990). New correlation of roughness density effect on the turbulent boundary layer. *AIAA Journal*. 28 (3): 554–556. <https://doi.org/10.2514/3.10427>
- Spuhler T., Kellersmann A., Bode C., Friedrichs J., Reitz G., et al. (2019). *The V2500-A1 as a Test Rig towards Digital Twin Modeling*. International Gas Turbine Congress.
- Sridhar M., Sunnam S., Goswami S., and Liu J. S. (2011). CFD aerodynamic performance validation of a two-stage high pressure turbine. *Turbo Expo: Power for Land, Sea, and Air*, pp. 1175–1184. <https://doi.org/10.1115/GT2011-45569>
- Tarabrin A. P., Schurovsky V. A., Bodrov A. I., and Stalder J. P. (1998). Influence of Axial Compressor Fouling on Gas Turbine Unit Performance Based on Different Schemes and With Different Initial Parameters. In: *Volume 4: Heat Transfer; Electric Power; Industrial and Cogeneration*. ASME, p. V004T11A006. <https://doi.org/10.1115/98-GT-416>
- Ulrich C. (2019). Numerische Kennfeldberechnung einer Flugtriebwerks-Niederdruckturbine. Bachelor thesis, Leibniz University Hannover.
- Vieweg M., Wolters F., and Becker R. G. (2017). Comparison of a heat soakage model with turbofan transient engine data. *ASME Turbo Expo 2017: Turbomachinery Technical Conference and Exposition*. <https://doi.org/10.1115/GT2017-63461>
- Wensky T., Winkler L., and Friedrichs J. (2010). Environmental influences on engine performance degradation. *Turbo Expo: Power for Land, Sea, and Air*, pp. 249–254. <https://doi.org/10.1115/GT2010-22748>
- Wilcox D. C. (1988). Reassessment of the scale-determining equation for advanced turbulence models. *AIAA Journal*. 26 (11): 1299–1310. <https://doi.org/10.2514/3.10041>
- Wolters F., Becker R., Schnell R., and Ebel P. B. (2016). Engine performance simulation of the integrated V2527-Engine Fan. In *54th AIAA Aerospace Sciences Meeting*, p. 388. <https://doi.org/10.2514/6.2016-0388>